DEUTSCHES ELEKTRONEN-SYNCHROTRON DESY

DESY 79/63
October 1979

HEAVY QUARKS IN e^+e^- ANNIHILATION

by

A. Ali, J. G. Körner
Deutsches Elektronen-Synchrotron DESY, Hamburg

G. Kramer, J. Willrodt
II. Institut für Theoretische Physik der Universität Hamburg

NOTKESTRASSE 85 - 2 HAMBURG 52

To be sure that your preprints are promptly included in the
HIGH ENERGY PHYSICS INDEX ,
send them to the following address (if possible by air mail) :

DESY
Bibliothek
Notkestrasse 85
2 Hamburg 52
Germany

DESY 79/63
October 1979

Heavy Quarks in e^+e^- Annihilation

A. Ali, J.G. Körner

Deutsches Elektronen-Synchrotron DESY, Hamburg

G. Kramer, J. Willrodt

II. Institut für Theoretische Physik der Universität Hamburg [+)]

[+)] Supported by Bundesministerium für Forschung und Technologie, Federal Republic of Germany.

Abstract

We calculate the effects of the pair production of top quarks and their subsequent weak decays on event topologies and inclusive distributions in e^+e^- annihilation experiments. The resulting jet distributions are compared with those originating from the lighter quarks (u,d,s,c,b) with higher order QCD corrections included.

The calculation is based on the Kobayashi-Maskawa model for the weak decay of the heavy quarks including nonleptonic and semileptonic decay modes. The final evolution of quarks into hadrons has been taken into account using a quark fragmentation model.

We find that the jet measures such as sphericity, thrust and acoplanarity are very sensitive to the onset of a new quark threshold in e^+e^- experiments. A comparison is made with available data from PETRA in the energy range $13 \leq E_{cm} \leq 31.6$ GeV in order to test the model below the $t\bar{t}$ production threshold.

I. Introduction

Recent experiments have shown that the hadronic final states in e^+e^- annihilation consist predominantly of two back-to-back jets at center-of-mass energies (E_{cm}) larger than 5 GeV [1-4]. These jets are characterized by a limited transverse momentum of the hadrons in the jet relative to the jet axis with a $\langle p_T \rangle \simeq 0.3$ GeV [2,3] and a jet angular distribution of $\sim(1 + \cos^2\theta)$ relative to the e^+e^- beam direction.

Quantum Chromodynamics (QCD) provides a basic explanation of this two-jet structure: To zeroth order in the quark gluon coupling constant α_s, the annihilation proceeds via a quark-antiquark pair creation. At short distances the quarks behave as if they were free and the $(1 + \cos^2\theta)$ distribution of the jet axis is expected for the point-like production of a pair of massless spin 1/2 particles. At long distances quarks are confined and hence must fragment into ordinary hadrons. This fragmentation process produces the limited transverse momentum with respect to the jet axis and is responsible for the observed Feynman inclusive hadron momentum distribution.

When a new flavour threshold is crossed the topology of events is expected to change. Close to the threshold, the $Q\bar{Q}$ pair production is dominated by heavy meson ($H\bar{H}$, $H\bar{H}^*$ etc.) pair production, and the heavy hadrons have relatively small momentum. The H decay weakly through the dominant mechanism ($H = Q\bar{q}$)

$$Q \to q' \ell^\pm \nu_\ell$$
$$Q \to q' q \bar{q} \qquad (1.1)$$

Depending upon the form of the weak current and the mass, the quark q' may decay further thus giving rise to almost spherical distributions near the $Q\bar{Q}$ threshold with a large accompanying multiplicity. Weak decays generate large p_T ($\langle p_T \rangle_{q'}^{weak} \sim \frac{1}{3}(m_Q - m_{q'})$, so $\langle p_T \rangle$, and all measures of $\langle p_T \rangle$, will show an increase as a new quark threshold is crossed. The large p_T, originating essentially from large m_Q, will persist even at energies much above the threshold. Since for heavy quarks the jet spread is roughly determined by $\delta_{weak} \sim \frac{(p_T)_{weak}}{(p_{||})_Q} \sim \frac{m_Q}{E_{cm}}$ as compared to the non-perturbative spread, $\delta_{nonpert} \sim \frac{(p_T)_{nonpert}}{(p_{||})_q} \sim \frac{\ln E_{cm}}{E_{cm}}$ heavy quark jets will certainly be broader as compared to the jets originating from the $u\bar{u}$, $d\bar{d}$ and $s\bar{s}$ quarks at subasymptotic energies. Of course, also until asymptotic energies the Feynman x and the θ distributions will change due to heavy $Q\bar{Q}$ production.

The changes in event topology can be studied quantitatively through the measurement of scalar jet quantities which have recently been proposed to characterize the "jettiness" of events. Among these are sphericity $\hat{S}$ [5], spherocity S [6], thrust T [7] and acoplanarity A [8].

In a recent paper we presented some results on differential $\hat{S}$ and T distributions as well as on the q^2-dependence of $\langle \hat{S} \rangle$ and $\langle 1-T \rangle$ above the threshold for charm, bottom and top quark production [9]. A careful and thorough investigation of these effects is important for several reasons. First, a quantitative study of these effects might help to locate new heavy quark thresholds. Second, a reliable test of genuine higher order QCD processes $e^+e^- \to q\bar{q}g$, $q\bar{q}gg$ and $q\bar{q}q\bar{q}$, which, as it seems, show up at PETRA energies ($\gtrsim 27$ GeV) [10], calls for a careful investigation of the background

generated by weakly decaying heavy quarks. Third, by disentangling the weak decay processes from the perturbative QCD processes one can perhaps gain some insight into the properties of the mechanism that governs the decay of the heavy quarks. In the PETRA energy range one thus has basically three kinds of sources for final hadron production. First, there is the lowest order $q\bar{q}$ production process of u, d and s quark pairs. These are dressed with phenomenologically calculable nonperturbative effects that are responsible for the transformation of quarks into hadrons and give rise to a nonperturbative 2-jet structure. Second, one has the genuine higher order perturbative QCD-processes $q\bar{q}g$, $q\bar{q}gg$ etc. which involve nonperturbative effects in the hadronisation process again. Third, one has the production and weak decay of heavy quark pairs $t\bar{t}$, $b\bar{b}$, $c\bar{c}$. The distributions due to this mechanism are also expected to be influenced by nonperturbative effects in the production and decay process. Whereas the first and third phenomena have jet spreads which decrease as $\ln E_{cm}/E_{cm}$ the QCD processes behave like powers of $\alpha_s(E_{cm}^2) \sim \ln^{-1}(E_{cm})$. Therefore the perturbative QCD processes will eventually dominate over the nonperturbative and weak decay effects at high enough energies if the opening of new quark thresholds does not continue ad infinitum. All this has been already observed in the recent high energy experiments at PETRA [10].

In the present paper we consider all these three phenomena with particular emphasis on the energy range 10 GeV $\lesssim E_{cm} \lesssim$ 40 GeV. We extend the results of [9] by including the weak cascade chains

and

In addition to sphericity and thrust we present distributions for acoplanarity and the single inclusive cross section $d\sigma/dp_T$, $d\sigma/dx$ and $d\sigma/dE_\ell$ (where E_ℓ is the lepton energy). We also calculate multiplicity distributions for charged hadrons and leptons.

The nonperturbative background from (u,d,s) jets is estimated using the Field-Feynman Monte Carlo program [11]. For the jets originating from the heavy quarks we have developed a new Monte Carlo program which will be described in the next section.

To test our model we compare it with recently published data from the TASSO and the MARK J collaborations at PETRA [10,12]. We have included also the QCD corrections from 3 jet and 4 jet configurations ($q\bar{q}g$, $q\bar{q}gg$ and $q\bar{q}q\bar{q}$) since they also lead to broadening effects and therefore must be taken into account if one wants to calculate the effect of the $t\bar{t}$ threshold. A detailed description of the QCD effects and further comparison with experimental data will be presented elsewhere [13]. A detailed discussion and description of the QCD 4 jet processes have been presented already in ref. 14.

We concentrate in this paper on the heavy quark jets and the jet-broadening

at high E_{cm} due to weak interactions, in particular those originating from the top quark decay. The weak interaction effects near the $b\bar{b}$ threshold have been studied already in our earlier work [15].

The paper is organized as follows. In section 2 we give a brief description of our basic formula for the production and decay of heavy quarks and discuss our method of computation. This section also includes a discussion of the fragmentation of quarks which takes place after the weak decays and the choice of the fragmentation function for heavy quarks. In section 3 we present distributions in thrust, sphericity, acoplanarity as well as single inclusive cross sections for E_{cm} = 36 GeV and results for average quantities as a function of E_{cm} for the processes $e^+e^- \to q\bar{q}$ with 4 quarks (u,d,s,c), 5 quarks (u,d,s,c,b) and 6 quarks (u,d,s,c,b,t) including QCD corrections due to $e^+e^- \to q\bar{q}g$, $q\bar{q}gg$ and $q\bar{q}q\bar{q}$. The value E_{cm} = 36 GeV was chosen since no top effects have been seen at lower energies ($E_{cm} \lesssim 32$ GeV) [12]. The model is tested by comparing these average quantities with available experimental data [10,12]. Section 4 contains a summary of our results [16].

II. Jet Distributions from Heavy Quark Decay

Our basic framework for the weak decays of charm, bottom and top quarks is the current x current interaction with the charged currents given by the Kobayashi-Maskawa (KM) model [17]. The dominant hadronic transitions for the decay of the c, b and t quark in the KM model are expected to be the following [9,18]:

$$c \to s + u + \bar{d} \tag{2.1a}$$

$$b \to c + d + \bar{u} \tag{2.1b}$$

$$b \to c + s + \bar{c} \tag{2.1c}$$

$$t \to b + u + \bar{d} \tag{2.1d}$$

$$t \to b + \bar{s} + c \tag{2.1e}$$

After the production of a heavy quark pair the heavy quarks will eventually fragment into a number of light hadrons and the lightest heavy meson of its species (or with much less probability into the lightest heavy baryon) which will then decay weakly.

The hadronic weak decays of the lightest heavy meson can proceed by the two mechanisms depicted in Fig. 1a and 1b (annihilation of the heavy and light quarks in the heavy hadron $H = Q\bar{q}$, producing two new light quarks) and Fig. 1c (decay of the heavy quark Q with the antiquark $\bar{q}$ acting as a spectator). The decays in Fig. 1a and 1b can be interpreted, for large m_Q, as two jet decays and those in Fig. 1c as three jet decays. In ref. 9 we computed the 2 jet/3 jet ratios for the bottom and top mesons and found the 3 jet channels to be dominant in all cases. For the $(b\bar{c})$ and $(t\bar{b})$ mesons, the 2 jet decay channel is not negligible. However, we continue to neglect the 2 jet modes since $(b\bar{c})$ and $(t\bar{b})$ mesons are not expected to be produced copiously.
We base our calculations on the modes (2.1b,c) for bottom decays and (2.1d,e) for top decays. Thus we will discuss the following decay chains:

(i) $c\bar{c}$-production:

$$c \to s + u + \bar{d} \tag{2.2}$$

For $b\bar{b}$-production:

$$b \to c + d + \bar{u}, \qquad \text{and} \qquad b \to c + s + \bar{c}$$
$$\hookrightarrow s + u + \bar{d} \qquad\qquad \hookrightarrow \bar{s} + \bar{u} + d$$
$$\hookrightarrow s + u + \bar{d}$$

(ii) $t\bar{t}$-production:

Here we have different possibilities. Two of them are:

$$t \to b + \bar{d} + u, \qquad t \to b + c + \bar{s} \tag{2.3}$$
$$\hookrightarrow c + d + \bar{u}, \qquad\qquad \hookrightarrow s + u + \bar{d}$$
$$\hookrightarrow s + u + \bar{d} \qquad\qquad \hookrightarrow c + s + \bar{c},$$
$$\hookrightarrow \bar{s} + \bar{u} + d,$$
$$\hookrightarrow s + u + \bar{d}$$

We have not listed all possible branches in (2.3) for reasons of brevity. Also $u+\bar{d}$ can be replaced by leptons $\ell + \bar{\nu}_\ell$, where $\ell = e, \mu$ or τ (if kinematically possible).

We have assumed the following quark masses

$$\begin{aligned} m_t &= 15.0 \text{ GeV} \\ m_b &= 5.0 \text{ GeV} \\ m_c &= 1.8 \text{ GeV} \\ m_s &= 0.5 \text{ GeV} \end{aligned} \tag{2.4}$$

and have neglected the u and d quark masses.

The production process $e^+e^- \to Q\bar{Q}$ is given by the lowest order one-photon exchange diagram and is described by the Lorentz-invariant density matrix element:

$$|\mathcal{M}|^2 = \frac{\alpha^2}{q^4}\left\{(\ell_+ p_1)(\ell_- p_2) + (\ell_+ p_2)(\ell_- p_1) + m_Q^2 q^2/4\right\} \tag{2.5}$$

where ℓ_- (ℓ_+) is the electron (positron) four-momentum and $p_1(p_2)$ is the four-momentum of the heavy quark $Q(\bar{Q})$. $q = (p_1 + p_2) = (\ell_- + \ell_+)$ and m_Q is the heavy quark mass.

The dynamics of the dominant 3-jet decay process

$$Q(p) \to q_1(q_1) + \bar{q}_2(q_2) + q_3(q_3) \tag{2.6}$$

is computed from the following Lorentz-invariant density matrix element according to a (V-A) interaction [9]:

$$|\mathcal{M}|^2 = G_F^2 (q_1 \cdot q_3)(p \cdot q_2) \qquad \text{(c- and t-quark)} \tag{2.7}$$

and

$$|\mathcal{M}|^2 = G_F^2 (q_1 \cdot q_2)(p \cdot q_3) \qquad \text{(b-quark)} \tag{2.8}$$

where G_F is the Fermi Coupling Constant $G_F = 1.02 \times 10^{-5} m_p^{-2}$. One has also to take into account the effect that the heavy quark looses some of its longitudinal momentum prior to its weak decay by fragmenting off ordinary hadronic matter. We have calculated this fragmentation of a heavy quark into hadrons and a heavy meson by using a generalized Field-Feynman like Monte Carlo model [11]. Ordinary hadrons are produced with a primordial quark

fragmentation function

$$f(z) = 1 - a + 3a(1-z)^2 \qquad (2.9)$$

with $z = p_h/p_q$ and $a = 0.77$ and an exponential p_T-distribution with an average $\langle p_T \rangle_q$ of 300 MeV.

However, the fragmentation function for the heavy quark into a heavy meson is expected to differ from (2.9). It is generally believed that the meson $H = (Q\bar{q})$ into which the heavy quark Q fragments carries the bulk of the parent quark momentum. Such a picture is also supported by the inclusive lepton measurements in ν-dimuon [19] and e^+e^- colliding beam experiments [20] where the experimental data favour

$$D_c^H(z) = (1-z)^n \text{ with } 0 \lesssim n \lesssim 1 \qquad (2.10)$$

On the other hand Bjorken [21] has argued that for super heavy quarks one anticipates

$$\langle z_H \rangle = 1 - (1\,\text{GeV})/m_Q \qquad (2.11)$$

A realistic fragmentation function for the b and t quarks is presumably given by

$$D_Q^H(z) = z^n \qquad n = 0,\ 1 \qquad (2.12)$$

The calculations presented in this paper are done assuming n = 1 in (2.10) and 0 in (2.12). However, to show the sensitivity of the various jet distributions

to the fragmentation function we plot thrust distribution at 9.4 GeV for the choice n = 0, 1 for charm fragmentation.

We have developed a Monte Carlo program in the spirit of the Field-Feynman Monte Carlo for the u,d,s quarks. In our model not only the quarks produced in the production step $e^+e^- \to Q\bar{Q}$ fragment into hadrons but so also do the quarks produced in the weak decays of the heavy quarks b and t. This is motivated by Bjorken's suggestion [21] that heavy quarks should produce a three jet structure of their own through semileptonic and nonleptonic decays. This independent quark decay picture is supported by recent calculations of the inclusive lepton energy distributions for the decay $c \to s + \ell + \bar{\nu}_\ell$ [22], which adequately describe the experimental data.

The appearance of jets in e^+e^- annihilation above $E_{cm} \gtrsim 6$ GeV sets the mass scale, where similar phenomenon should also occur in weakly decaying hadrons. In this context b decays seem to be on the border line. Consequently, we have modified our model to take that into account, as follows. Based on the free quark model matrix elements (2.7) and (2.8), we calculate the invariant mass distributions $\frac{d\Gamma}{ds_{13}}$ and $\frac{d\Gamma}{ds_{23}}$, where $s_{ij} = (q_i + \bar{q}_j)^2$. Only if both s_{13} and s_{23} are sufficiently large do we let the quarks fragment independently. In table 1 we list these cut-offs for the various b and t decay modes. The choice of these numbers is guessed by the hadronic continuum onset in e^+e^- annihilation and the masses of the hadrons that can couple to the $q_i\bar{q}_j$ system. There are thus the following processes involved in the decay of a heavy quark

$$\begin{aligned} Q &\to q \text{ jet} + \ell + \bar{\nu}_\ell \\ &\to 2 \text{ body} \\ &\to q \text{ jet} + \text{hadron} \\ &\to 2q \text{ jets} + \text{hadron} \\ &\to 3 \text{ q jets} \end{aligned} \qquad (2.13)$$

As m_Q increases the ratio of 2 body (and quasi two body) decays as well as the ratio for the process $Q \to q$ jet + hadron decreases, much the same way as in e^+e^- annihilation. The multiplicity in the decay of the bottom mesons thus is much smaller than the one naively expected from $\langle n_Q \rangle_{nonlept} = 3\langle n_q \rangle$ and is in the neighbourhood of the multiplicity $\langle n_b \rangle$ calculated for the b decays using a statistical isospin model [23].

Apart from this the fragmentation of the quarks produced in the weak decays is implemented in the same way as the Field-Feynman cascade model governed by the fragmentation function

$$f(z, p_T) \sim e^{-bp_T^2}(1 - a + 3a\eta^2) \qquad (2.14)$$

where $\eta = 1 - z$, $z = \frac{(E+p_\parallel)_h}{(E+p_\parallel)_q}$

with the same values for the parameters a and b as in the FF model.

For the relative rates for the various decay modes of the b and t decays, we again resort to the quark model (2.7) and (2.8). The phase space factor so obtained is combined with the assumption

$$\frac{\Gamma(Q \to q + \ell + \bar{\nu}_\ell)}{\Gamma(Q \to all)} = 0.1 \qquad (2.15)$$

where $Q = t, b, c$

$\ell = e, \mu, \tau$

The semileptonic branching ratio is again a guess based on the experimentally measured branching ratio for charm [24] and the nonleptonic enhancement calculation for the b and t quarks [18]. The assumed branching ratios so obtained are listed in table 2.

For charm decays, we have resorted to the particle data table [24] for the semi-leptonic decay modes. The bulk of the non-leptonic decay modes of charm are still unknown. We have randomly chosen the decay modes

$$D \to K\pi\pi \;,\; K^*\pi\pi \;,\; K\varrho\pi$$
$$F \to \eta\pi\pi \;,\; \eta'\pi\pi \;,\; \phi\pi\pi \;,\; K^*K$$

and used their phase space ratios to determine their relative weights, which again is calculated using the matrix element (2.7) but treating the quarks as hadrons with appropriate quantum numbers and masses. The resulting charge multiplicity, inclusive lepton and hadron energy spectrum, and the p_T distribution are in good agreement with the corresponding quantities measured experimentally in the region $3.77\ \text{GeV} \lesssim E_{cm} \lesssim 10.0\ \text{GeV}$.

Finally, all vectors and unstable pseudoscalar particles (η, η') are allowed to decay strongly using the particle data table and we are left with $\pi^\pm$, K^0, $K^\pm$, $\bar{K}^0$, γ, $e^\pm$, $\mu^\pm$ as the finally observed particles.

III. Results

Using the model described in the preceding section we now proceed to calculate differential distributions in sphericity $\hat{S}$, thrust T, acoplanarity A and various other quantities of interest, as for example p_T, p_{out}, multiplicity

etc., for the weak decays of the charm, bottom and top quarks in e^+e^- annihilation. We also compute the distributions coming from light (u,d,s) quark production and the QCD processes $e^+e^- \to q\bar{q}g$, $q\bar{q}gg$ and $q\bar{q}q\bar{q}$ including all quarks q = (u,d,s,c,b,t).

We have normalized our distributions (if not otherwise stated) for the heavy quarks according to the charge (square) formula:

$$\sigma(Q_a\bar{Q}_a)/\sigma_{tot} = \frac{e_a^2}{\sum_{a=1}^{n} e_a^2} \qquad (3.1)$$

The normalization and hence the contribution of higher order QCD processes to these distributions need some discussion. In general, the processes $e^+e^- \to q\bar{q}g$, $q\bar{q}gg$ and $q\bar{q}q\bar{q}$ are not well defined in the entire kinematic phase space due to the well known QCD singularities. In terms of thrust and acoplanarity this means that the $q\bar{q}g$ final state is singular for $T \to 1$ and the states $q\bar{q}gg$ and $q\bar{q}q\bar{q}$ are singular for $A \to 0$. Since the process $e^+e^- \to q\bar{q}g$ is not reliably calculable in the limit $T \to 1$ and likewise $\sigma_{q\bar{q}gg}$ and $\sigma_{q\bar{q}q\bar{q}}$ are not reliably calculable in the limit $A \to 0$ from the tree level diagrams alone we must introduce cut-offs T_0 and A_0 in such a way that the QCD processes are only taken into account for $T \leq T_0$ and $A \geq A_0$ respectively. A reasonable guess for the cuts T_0 and A_0 may be the ones which give $\sigma_{q\bar{q}g}/\sigma_0 \simeq \alpha_s$ and $\sigma_{(q\bar{q}gg + q\bar{q}q\bar{q})} \simeq \alpha_s^2$. This is suggestive though not compelling from the QCD corrections to σ_{tot}. We have chosen $T_0 = 0.95$ which gives $\sigma_{q\bar{q}g}/\sigma_0 = 33\ \%$ and $A_0 = 0.05$, corresponding to $\sigma_{(q\bar{q}gg + q\bar{q}q\bar{q})}/\sigma_0 = 6\ \%$, as cut offs to calculate

all QCD corrections. The gluons are then allowed to fragment into a $q\bar{q}$ pair, which fragment in turn. For details and discussion we refer to our later work [13].

Before we describe our final results we should perhaps still discuss the sensitivity of the heavy quark distributions on the heavy quark fragmentation function. In Fig. 2 we show the distribution $\frac{1}{\sigma}\frac{d\sigma}{dT}$ for charm production at $E_{cm} = 9.4$ GeV for the two fragmentation functions $D_c^D \sim (1-z)$ and $D_c^D \sim$ const. We see that the thrust distributions depend only marginally on $D_c^D(z)$ between these two choices. The sphericity distribution is even less sensitive in the above mentioned range of $D_c^D(z)$ and we refrain from showing this dependence. We remark, however, that $D_c^D(z) \sim \delta(1-z)$ produces a substantial difference in $\frac{1}{\sigma}\frac{d\sigma}{dT}$ compared to the $D_c^D(z) \sim$ const.

We shall concentrate mainly on the signatures of $t\bar{t}$ production in e^+e^- annihilation. To that end we present various distributions for three cases:

(i) $e^+e^- \to t\bar{t} \to$ hadrons + leptons
(ii) $e^+e^- \to (u\bar{u}, d\bar{d}, s\bar{s}, c\bar{c}, b\bar{b}) + g + gg \to$ hadrons + leptons
(iii) $e^+e^- \to (u\bar{u}, d\bar{d}, s\bar{s}, c\bar{c}, b\bar{b}, t\bar{t}) + g + gg \to$ hadrons + leptons

In Fig. 3 we show the distribution $\frac{1}{\sigma}\frac{d\sigma}{d\hat{s}}$ for all three cases mentioned above. In Fig. 4, we plot $\frac{1}{\sigma}\frac{d\sigma}{dT}$ and in Fig. 5 $\frac{1}{\sigma}\frac{d\sigma}{dA}$. In presenting these distributions we have chosen $E_{cm} = 36$ GeV and the top mass, $m_t = 15$ GeV. From these figures it is obvious that the onset of the top threshold will be signalled by a component with almost isotropic distributions. Note that this is a matter of general consequence and not specific to the particular model

used in this paper for quantitative estimates. It is clear that the higher the $t\bar{t}$ threshold lies the easier its detection will be by looking at any of the S, T and A distributions. We remark that the broadening of the distributions for the production of u,d,s,c and b quarks by single and double gluon emission is not strong enough to overcome the broadening caused by the production of additional $t\bar{t}$ pairs (compare for example the distributions in Figs. 3, Fig. 4 and Fig. 5). As we can see the effect seems to be largest in the T distribution. The distributions shown in Fig. 3, 4 and 5 are based on charged tracks only. Since most of the experimental setups at PETRA detect only charged particles these distributions are more useful at present.

Next we discuss the momentum distributions with respect to the axis perpendicular to the acoplanarity plane and w.r.t. the thrust axis. These distributions contain roughly the same information as the acoplanarity and the thrust distributions in Fig. 4 and 5. But because the variables are averages per event they are less dependent on changes of multiplicity. Therefore they make comparisons of data for different energies much easier. The exact definitions of these momentum averages are as follows. First

$$p_{out} = \frac{1}{N} \sum_{j=1}^{N} |\vec{p}_j \hat{n}_A| \qquad (3.2)$$

depending on the unit vector $\hat{n}_A$. $\hat{n}_A$ is the normal on the plane defined by minimal acoplanarity. The sum in (3.2) runs over all particles in an event (in our case only charged particles). Second

$$p_T = \frac{1}{N} \sum_{j=1}^{N} |\vec{p}_j \hat{n}_T| \qquad (3.3)$$

is the average momentum per event with respect to an axis $\hat{n}_T$ perpendicular to the thrust axis (transverse momentum). The p_{out} distributions are shown in Fig. 6 for all the three cases. Although the mean values of the distributions (ii)and (iii) do not differ very much the shape of the distributions for five and six quarks differ appreciably. The appearance of t quark is signalled by a long tail in the p_{out} distribution. The difference in the p_T distributions is somewhat less pronounced although still visible (see Fig. 7a,b,c). Here we show the distribution in p_T(high) and p_T(low) separately. p_T(high) and p_T(low) are the transverse momenta for the two sides of each event with respect to a plane perpendicular to the thrust axis. The motivation for this division comes from additional gluon emission. The "low" side should rarely have a noncollinear hard gluon. Of course, also without gluon emission the distribution in p_T(high) and p_T(low) differ due to statistical fluctuations (see Fig. 7a).

Next, we discuss the multiplicity distribution for charged particles. In Fig. 8a we show the fraction of events as a function of n_{ch} for $t\bar{t}$ production alone. The average of this distribution is $\langle n_{ch} \rangle = 21.4$. Without any $t\bar{t}$ contribution the multiplicity distribution is given in Fig. 8b with $\langle n_{ch} \rangle = 14.0$ The combined distribution with all six quarks is in Fig. 8c. The average is $\langle n_{ch} \rangle = 15.8$. Clearly this distribution is broader as compared to the distribution in Fig. 8b. It seems that the multiplicity distributions are also useful for detecting the top quark threshold. We remark that $\langle n_{ch} \rangle$ increases by ~ 2.0 units as the $t\bar{t}$ threshold is crossed.

In Figs. 9a,b,c we present the charged kaon multiplicity distribution for the three cases, mentioned already. Again the change in $\langle n_{K^\pm} \rangle$ as one crosses

the $t\bar{t}$ threshold is noticeable. This distribution is, however, based on the assumption (in the original FF model) that the ratio u:d:s = 2:2:1, and has not really been tested in contrast to $\langle n_c \rangle$ which we shall later compare with the data. It is obvious that both $\langle n_{ch} \rangle, \langle n_K^{+-} \rangle$ and the distributions $\frac{1}{\sigma}\frac{d\sigma}{dn_{ch}}$, $\frac{1}{\sigma}\frac{d\sigma}{dn_K}$ are tests of the Kobayashi-Maskawa model and hence are model dependent. The same is not true about the jet distributions shown in Figs. 3 - 7, which rely more on the mass of the top quark and that it decays almost isotropically giving rise to rather large multiplicities.

In Fig. 10 we plot the inclusive hadron distribution $S\frac{1}{\sigma}\frac{d\sigma}{dx}$ for the two cases: 5 quarks and 6 quarks. Note that in the absence of gluon bremsstrahlung this distribution is scale invariant. In order to have realistic background estimates we have included the gluon bremsstrahlung effects. The onset of the $t\bar{t}$ threshold results in the increase of the low x region - a feature well established from the $c\bar{c}$ and $b\bar{b}$ thresholds. However, since the gluon bremsstrahlung effect also go in the same direction the shift to lower values of x is not as pronounced as in the low energy data [25].

So far, we have confined ourselves to the discussion of the global properties of the $t\bar{t}$ production. A more sensitive test of the nature of the weak current, however, lies in the studies of leptons coming from the weak decays of the b and t quarks. It has long been pointed out in the literature that the shape of the lepton energy spectrum depends on the nature of the weak current [26]. It is clear that the cascade chain

$$t \to b + \ell + \bar{\nu}_\ell \quad , \quad b + \tau + \bar{\nu}_\tau \hookrightarrow \ell + \bar{\nu}_\ell$$
$$\hookrightarrow c + \ell + \bar{\nu}_\ell \quad , \quad c + \bar{c} + s$$
$$\hookrightarrow s + \ell + \bar{\nu}_\ell \quad \hookrightarrow \hookrightarrow s + \ell + \bar{\nu}_\ell$$

will lead to multilepton events, and consequently, the fraction of events containing leptons will increase significantly.

The shape of the lepton energy spectrum reflects, essentially, the hierarchy of quark masses [27]. In particular, there will be a very hard component in the spectrum coming from the primary decay

$$t \to b + \ell + \bar{\nu}_\ell$$

In Fig. 11, we plot the inclusive lepton energy spectrum as anticipated in the KM model both with and without a $t\bar{t}$ component. The difference in the shape of the two spectra is very noticeable, more so as it lies in the upper end of the spectrum thus surviving lepton energy cuts. In table 3, we present the inclusive cross section defined as

$$R(n\mu) = \frac{\sigma(e^+e^- \to n\mu + X)}{\sigma(e^+e^- \to all)}$$

We remark that the inclusive muon (and electron) rate increases by a factor 2 as the $t\bar{t}$ threshold is crossed. Fig. 13 can be used to extract more realistic numbers by determining the fraction of events surviving a given lepton energy cut. We point out that a cut-off of 1 GeV does not seriously dilute the $t\bar{t}$ component.

So far we offered no evidence that the model for the 5 quark production

which describes the background for the top search agrees reasonably well with the existing experimental data coming from DORIS and PETRA. This will be done in a separate publication [13]. Here we compare only the average values of sphericity, thrust, spherocity, acoplanarity, p_{out}, p_T and n_{ch} with data taken at E_{cm} = 13, 17, 22, 27.5, 30 and 31.5 GeV (MARK J and TASSO at PETRA)(Fig. 12 and 13). We see that the overall agreement of our 5 quark model with these data is very satisfactory, showing that the top threshold has not been passed at these energies and that our treatment of QCD effects is correct. For the higher energies ($\gtrsim$33 GeV) the averages are shown for the 6 quark model (including QCD corrections). We emphasize that the threshold factor has not been taken into account so that the increase in $\langle 1-T \rangle$, $\langle \hat{S} \rangle$ etc. near the threshold is certainly overestimated outside resonances and underestimated just on top of a $t\bar{t}$ resonance. Also, the threshold energy (E_{cm} = 33 GeV) has no direct physical significance as well as the top mass value: m_t = 15 GeV, which is just an effective mass to characterize the region, where the $t\bar{t}$ resonance might occur. Similarly, the discontinuity at E_{cm} = 12.5 GeV in $\langle \hat{S} \rangle$, $\langle 1-T \rangle$ etc. is the effect of the bottom threshold. Here again, this threshold energy is an effective value. The question whether the available experimental data at E_{cm} = 13 and 17 GeV indicate already the threshold for open bottom production was considered already in ref. 15. In Fig. 13 we plotted the average transverse momenta $\langle p_T \rangle_T$, $\langle p_T(\text{low}) \rangle_T$, $\langle p_T(\text{high}) \rangle_T$ where p_T is measured with respect to the thrust axis and $\langle p_T \rangle_S$ where p_T is determined relative to the sphericity axis and the average $\langle p_{out} \rangle$ where p_{out} is determined relative to the acoplanarity plane. These quantities are rather constant as a function of energy. The steps due to the $t\bar{t}$ threshold are not very dramatic. Of course,

the small increase of $\langle p_T \rangle$ and $\langle p_{out} \rangle$ is the effect of the gluon emission, which due to the cuts in thrust and acoplanarity is very much reduced compared to older predictions [28]. We notice that the agreement with the data of the TASSO collaboration is very satisfactory, showing again that our model for the background is realistic.

As the last point we mention a comparison of the average charged particle multiplicity $\langle n_{ch} \rangle$ with the TASSO data. In our 5-quark model with QCD corrections the $\langle n_{ch} \rangle$ has the following values $\langle n_{ch} \rangle$ = 8.5, 9.8, 11.2, 12.3, 12.8 and 13.2 at E_{cm} = 13, 17, 22, 27.6, 30 and 31.6 GeV. These numbers agree reasonably well with the measured values at the same energies. The experimental numbers for $\langle n_{ch} \rangle$ are: 7.8 ± 1.0, 8.6 ± 1.0, 9.5 ± 1.0, 10.8 ± 1.0, 11.7 ± 1.0 and 11.4 ± 1.0. This agreement with the experimental values of $\langle n_{ch} \rangle$ is important since only then the calculated distributions in thrust, sphericity etc. describe the same physics. On the other hand the nice agreement of $\langle T \rangle$, $\langle \hat{S} \rangle$ etc. on one side and of $\langle p_T \rangle$, $\langle p_{out} \rangle$ etc. on the other side with the experimental data indicates that also the multiplicity must come out in agreement with the measured data.

IV. Summary and Conclusions

We have calculated the effect of heavy quark production and their subsequent weak decays on the various jet distributions measured in e^+e^- annihilation experiments. The detailed distributions are based on the dominance of the transitions $t \to b$, $b \to c$ and $c \to s$. Based on this chain one gets a 14, 10 and 6 quark final state in the production of $t\bar{t}$, $b\bar{b}$ and $c\bar{c}$ respectively. The final evolution of all these quarks into hadrons was calculated with a

Feynman-Field type fragmentation model. Semileptonic decay modes were included.

We studied in detail the effect that the production of additional heavy quark-anti-quark pairs with Q = 2/3 would have on the distributions in jet measures like $\hat{S}$, T and A. It was found that these distributions and their average values are much more sensitive probes of detecting new quark thresholds in e^+e^- annihilation than the value of R. We have presented detailed distributions in these variables and in various transverse momenta for the anticipated $t\bar{t}$ production for a representative value of m_t (15 GeV) and E_{cm} (36 GeV). These distributions are compared with the distributions coming from the pair production of the known quarks u,d,s,c and b. We included QCD corrections coming from single and double gluon bremsstrahlung. The model with five quarks and additional gluons was compared with recent data from the TASSO and MARK J collaborations at PETRA. The agreement was rather satisfactory showing that the description of the fragmentation process for the old quarks including gluon emission is realistic.

Acknowledgement

We are grateful to the members of the MARK J, PLUTO and TASSO groups for numerous interesting discussions regarding the experimental data. In particular we thank H. Newman, T. Meyer and G. Wolf for communication of some results prior to publication.

References

1 G.G. Hanson et al., Phys. Rev. Lett. 35 (1975) 1609

2 Ch. Berger et al., Phys. Lett. 78B (1978) 176

3 G.G. Hanson, SLAC preprints SLAC-PUB 1814 (1976) and SLAC-PUB 2118 (1978) and Proceedings of the 13th Rencontre de Moriond on High Energy Leptonic Interactions and High Energy Hadronic Interactions, Les Arcs, March 12-24, 1978.

4 Ch. Berger et al., Phys. Lett. 82B (1979) 449

5 J.D. Bjorken, S.J. Brodsky, Phys. Rev. D1 (1970) 1416, G. Parisi, Phys. Lett. 74B (1978) 65

6 H. Georgi, M. Machacek, Phys. Rev. Lett. 39 (1977) 1237

7 E. Fahri, Phys. Rev. Lett. 39 (1977) 1587; see also S. Brandt et al., Phys. Lett. 12 (1964) 57; S. Brandt, H.D. Dahmen, Z. Physik C, Particles and Fields, 1 (1979) 61

8 A. de Rújula, J. Ellis, E.G. Floratos, M.K. Gaillard, Nucl. Phys. B138 (1978) 387

9 A. Ali, J.G. Körner, G. Kramer and J. Willrodt, Z. Physik C, Particles and Fields, 1 (1979) 203

10 See for example: TASSO Collaboration, R. Brandelik et al., DESY preprint, DESY 79/53; D.P. Barber et al., MIT preprints, Report No. 105, 106 ; PLUTO Collaboration, Ch.Berger et al., DESY Preprint DESY 79/57

11 R.D. Field and R.P. Feynman, Nucl. Phys. B136 (1978) 1

12 See for example the reports of Ch. Berger, H. Newman, S. Orito and G. Wolf at the Photon-Hadron Conference, FNAL, Chicago, 1979

13 A. Ali, E. Pietarinen, G. Kramer and J. Willrodt, to be published

14 A. Ali, J.G. Körner, Z. Kunszt, J. Willrodt, G. Kramer, G. Schierholz, E. Pietarinen, Phys. Lett. 82B (1979) 285,
A. Ali, J.G. Körner, Z. Kunszt, E. Pietarinen, G. Kramer, G. Schierholz and J. Willrodt, DESY preprint, DESY 79/54

15 A. Ali, J.G. Körner, J. Willrodt and G. Kramer, Phys. Lett. 83B (1979) 375

16 Results based on the model described in this paper relevant for the top search have been presented already earlier in various talks by the authors. See also: G. Flügge, DESY report, DESY 79/26,
H. Spitzer, Internal Report, DESY PLUTO-79/03

17 M. Kobayashi, K. Maskawa, Prog. Theor. Phys. 49 (1973) 652

18 J. Ellis, M.K. Gaillard, D.V. Nanopoulos and S. Rudaz, Nucl. Phys. B131 (1977) 285

19 R. Odorico, Phys. Lett. 71B (1971) 121

20 Lead Glass Wall Collaboration, Report to XIX International Conference on High Energy Physics, 1978, Tokyo, Japan

21 J.D. Bjorken, Phys. Rev. D17 (1978) 171

22 A. Ali and E. Pietarinen, Nucl. Phys. B154 (1979) 519,
N. Cabibbo and L. Maiani, Phys. Lett. 79B (1978) 109

23 A. Ali, J.G. Körner, G. Kramer and J. Willrodt, Z. Physik C, Particles and Fields, 2 (1979) 34

24 Particle Data Group, Phys. Lett. 75B (1978) 1

25 See for example the review article by B. Wiik and G. Wolf, DESY report (1978), unpublished

26 A. Ali and T.C. Yang, Phys. Lett. 65B (1976) 275

27 For the details of semileptonic decay distributions and relevant formulae, see A. Ali, Z. Physik C, Particles and Fields 1 (1979) 25

28 G. Kramer and G. Schierholz, Phys. Lett. 82B (1979) 208

Figure Captions

Fig. 1: Jet decays of weakly decaying heavy mesons: a), b) two jet decay and c) three jet decay.

Fig. 2: Influence of fragmentation function D_c^D on the thrust-distribution $\frac{1}{\sigma}\frac{d\sigma}{dT}$ at E = 9.4GeV. Solid curve is $D_c^D = 2(1-z)$, dashed curve is D_c^D = const., dash-dotted curve is the charm contribution ($D_c^D = 2(1-z)$), dash-doubly-dotted curve is the charm contribution for D_c^D = const.

Fig. 3: Sphericity distribution $\frac{1}{\sigma}\frac{d\sigma}{d\hat{S}}$ at E_{cm} = 36 GeV and with m_t = 15 GeV for $t\bar{t}$ production (dashed), 5 quarks plus QCD corrections (dash-dotted) and 6 quarks plus QCD corrections (solid).

Fig. 4: Thrust distribution $\frac{1}{\sigma}\frac{d\sigma}{dT}$, see Fig. 3 for description of curves.

Fig. 5: Acoplanarity distribution $\frac{1}{\sigma}\frac{d\sigma}{dA}$, see Fig. 3 for description of curves.

Fig. 6: p_{out} distribution $\frac{1}{\sigma}\frac{d\sigma}{dp_{out}}$, see Fig. 3 for description of curves.

Fig. 7: p_T distributions $\frac{1}{\sigma}\frac{d\sigma}{dp_T}$ for p_T(high) and p_T(low) separately. (a) only $t\bar{t}$ production, (b) 5 quarks plus QCD corrections, (c) 6 quarks plus QCD corrections.

Fig. 8: Charged particle multiplicity distribution with m_t = 15 GeV at E_{cm} = 36 GeV for (a) $t\bar{t}$ production, (b) 5 quarks plus QCD, (c) 6 quarks plus QCD.

Fig. 9: Charged K-meson multiplicity distribution, (a), (b) and (c) as in Fig. 8.

Fig. 10: Inclusive hadron distribution $\frac{1}{\sigma}\frac{d\sigma}{dx}$ for 5 quarks plus QCD corrections (solid curve) and 6 quarks plus QCD corrections (dashed curve) at E_{cm} = 36 GeV.

Fig. 11: Inclusive lepton energy spectrum for E_{cm} = 36 GeV, m_t = 15 GeV.

Fig. 12: Average jet measures $\langle T\rangle$, $\langle\hat{S}\rangle$, $\langle S\rangle$ and $\langle A\rangle$ as a function of E_{cm} for 5 quarks (dashed-dot), 5 quarks plus QCD (full) and 6 quarks plus QCD (dashed) compared to experimental data of the TASSO and MARK J group at PETRA [10,12]

Fig. 13: Average quantities $\langle p_T\rangle_T$, $\langle p_T(\text{low})\rangle_T$, $\langle p_T(\text{high})\rangle_T$, $\langle p_T\rangle_S$ and $\langle p_{out}\rangle$ as a function of E_{cm} compared to experimental data of the TASSO group at PETRA [10,12], distinction of curves see Fig. 12.

Table Captions

Table 1: Values of the cut-off on the invariant masses of the $q\bar{q}$ system in the non-leptonic decays of t and b quarks.

Table 2: Branching ratios for the various semileptonic and nonleptonic decay modes of the b and t quarks derived from the quark model phase space and non-leptonic enhancement factors.

Table 3: The ratio $R = \frac{\sigma(e^+e^- \to \mu + X)}{\sigma(e^+e^- \to all)}$ for the various multilepton states with and without the $t\bar{t}$ production.

Decay Modes	cut-off $[GeV^2]$
$b \to c\bar{u}d$	$\Lambda^2_{\bar{u}d} = 2.25$ $\Lambda^2_{\bar{u}c} = 6.25$
$b \to c\bar{c}s$	$\Lambda^2_{c\bar{c}} = 14.25$ $\Lambda^2_{s\bar{c}} = 6.25$
$t \to bu\bar{d}$	$\Lambda^2_{u\bar{d}} = 2.25$ $\Lambda^2_{b\bar{d}} = 30.0$
$t \to bc\bar{s}$	$\Lambda^2_{b\bar{s}} = 30.0$ $\Lambda^2_{c\bar{s}} = 2.25$

Table 1

Decay Modes	Branching Ratios
$b \to c\bar{u}d$	0.7
$b \to c\bar{c}s$	0.1
$b \to ce\bar{\nu}_e$ = $b \to c\mu\bar{\nu}_\mu$	0.1
$t \to bu\bar{d}$	0.4
$t \to bc\bar{s}$	0.32
$t \to be\bar{\nu}_e$ = $t \to b\mu\bar{\nu}_\mu$	0.1
$t \to b\tau\bar{\nu}_\tau$	0.08

Table 2

Branching Ratio	without $t\bar{t}$	with $t\bar{t}$	only $t\bar{t}$
$R(1\mu)$	0.103	0.174	0.234
$R(2\mu)$	0.007	0.034	0.053
$R(3\mu)$	4×10^{-4}	0.010	0.006
$R(4\mu)$	-	5.8×10^{-5}	0.002
$R(all\mu)$	0.11	0.218	0.294

Table 3

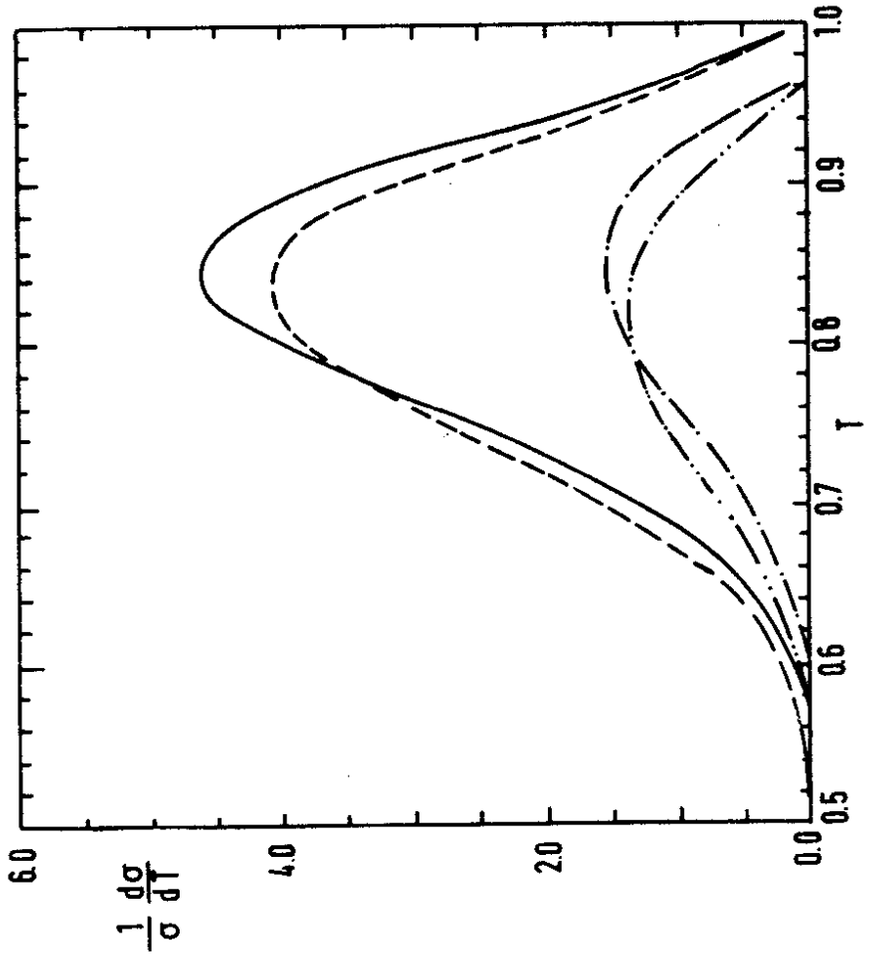
1.0
0.9
0.8
0.7
0.6
0.5
τ
6.0
4.0
2.0
0.0
$\frac{1}{\sigma}\frac{d\sigma}{d\tau}$

Fig.2

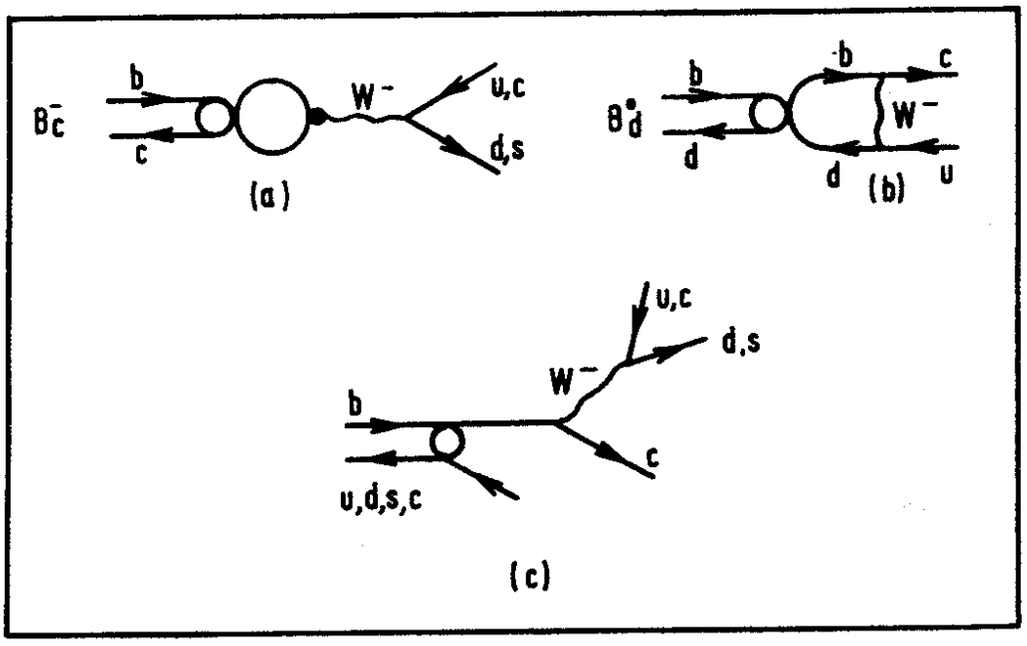
B_c^-
b
c
W⁻
u,c
d,s
(a)
B_d^0
b
d
b
c
W⁻
d
u
(b)
u,c
d,s
W⁻
b
c
u,d,s,c
(c)

Fig.1

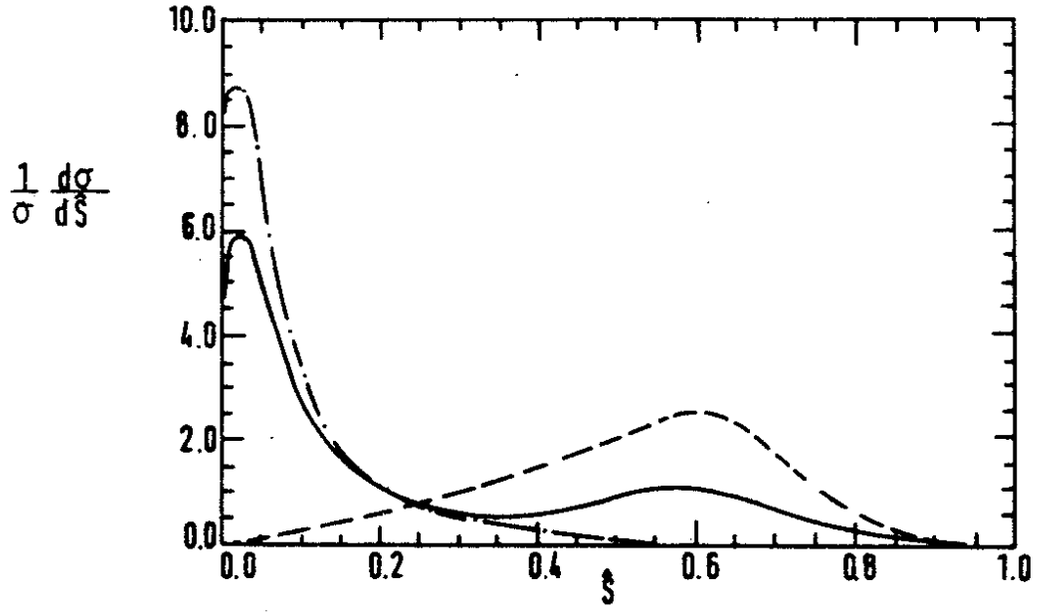
$\frac{1}{\sigma}\frac{d\sigma}{d\tilde{S}}$
10.0
8.0
6.0
4.0
2.0
0.0
0.0
0.2
0.4
0.6
0.8
1.0
$\tilde{S}$

Fig. 3

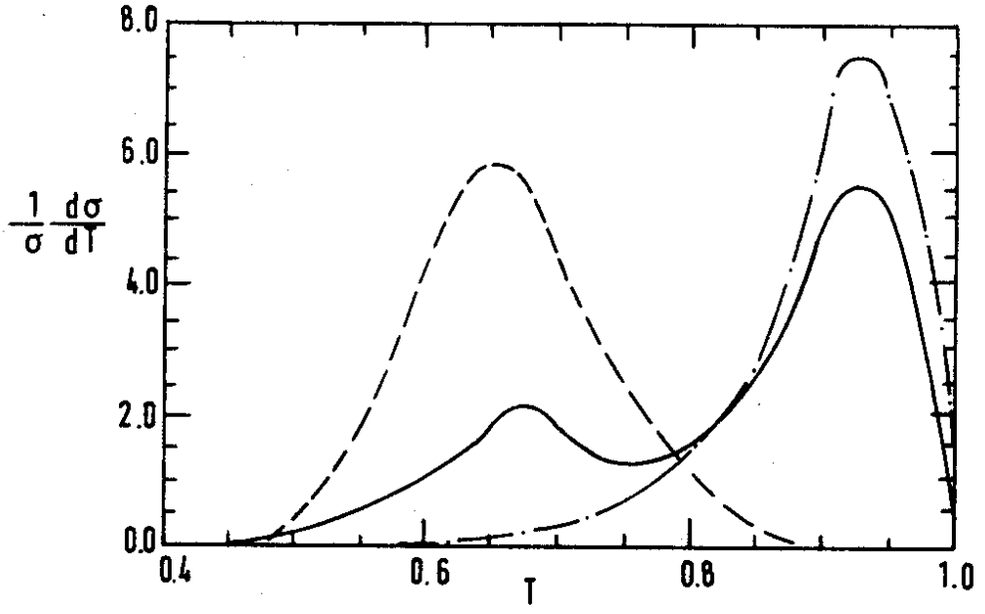
$\frac{1}{\sigma}\frac{d\sigma}{dT}$
8.0
6.0
4.0
2.0
0.0
0.4
0.6
0.8
1.0
T

Fig. 4

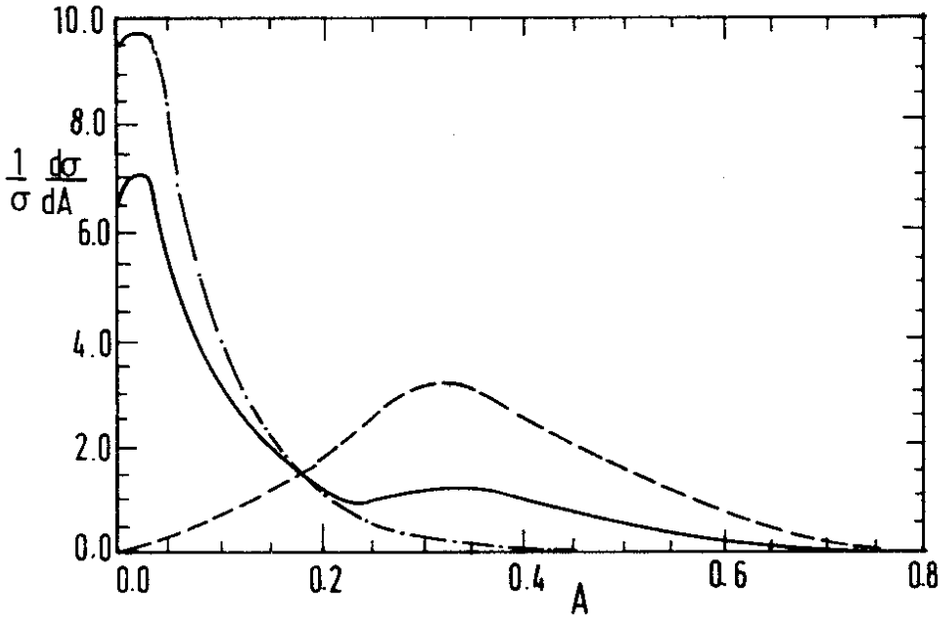
10.0
8.0
6.0
4.0
2.0
0.0
$\frac{1}{\sigma}\frac{d\sigma}{dA}$
0.0
0.2
0.4
0.6
0.8
A

Fig.5

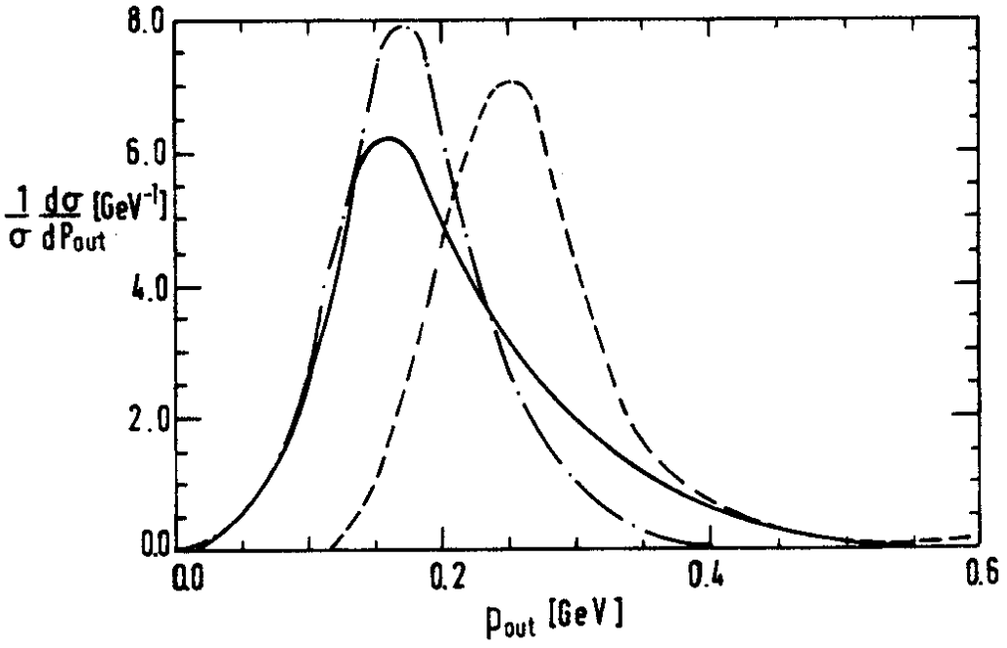
8.0
6.0
4.0
2.0
0.0
$\frac{1}{\sigma}\frac{d\sigma}{dP_{out}}$ [GeV^{-1}]
0.0
0.2
0.4
0.6
p_{out} [GeV]

Fig. 6

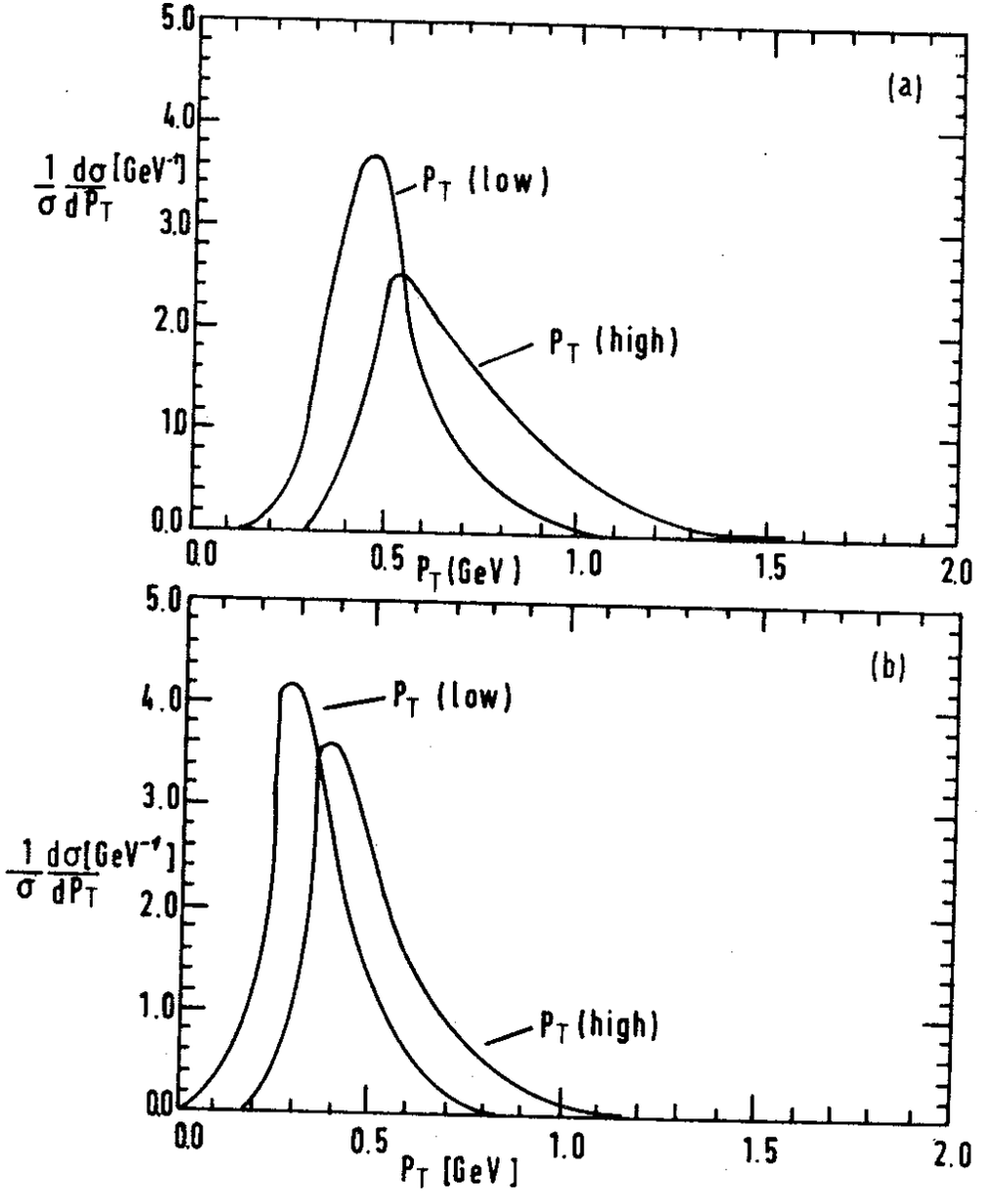

Fig. 7 a+b

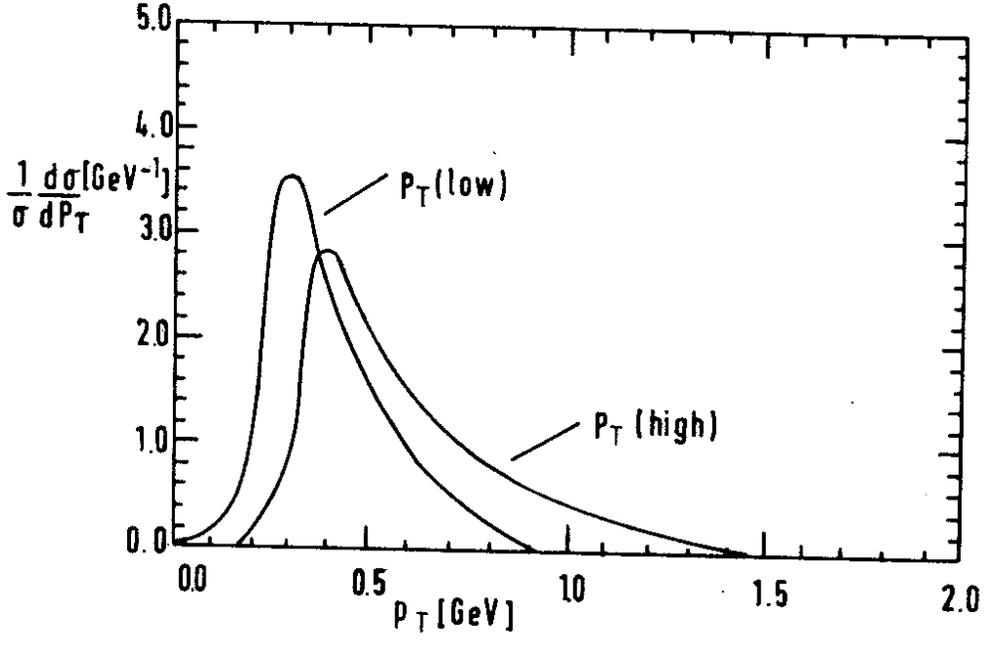

Fig. 7c

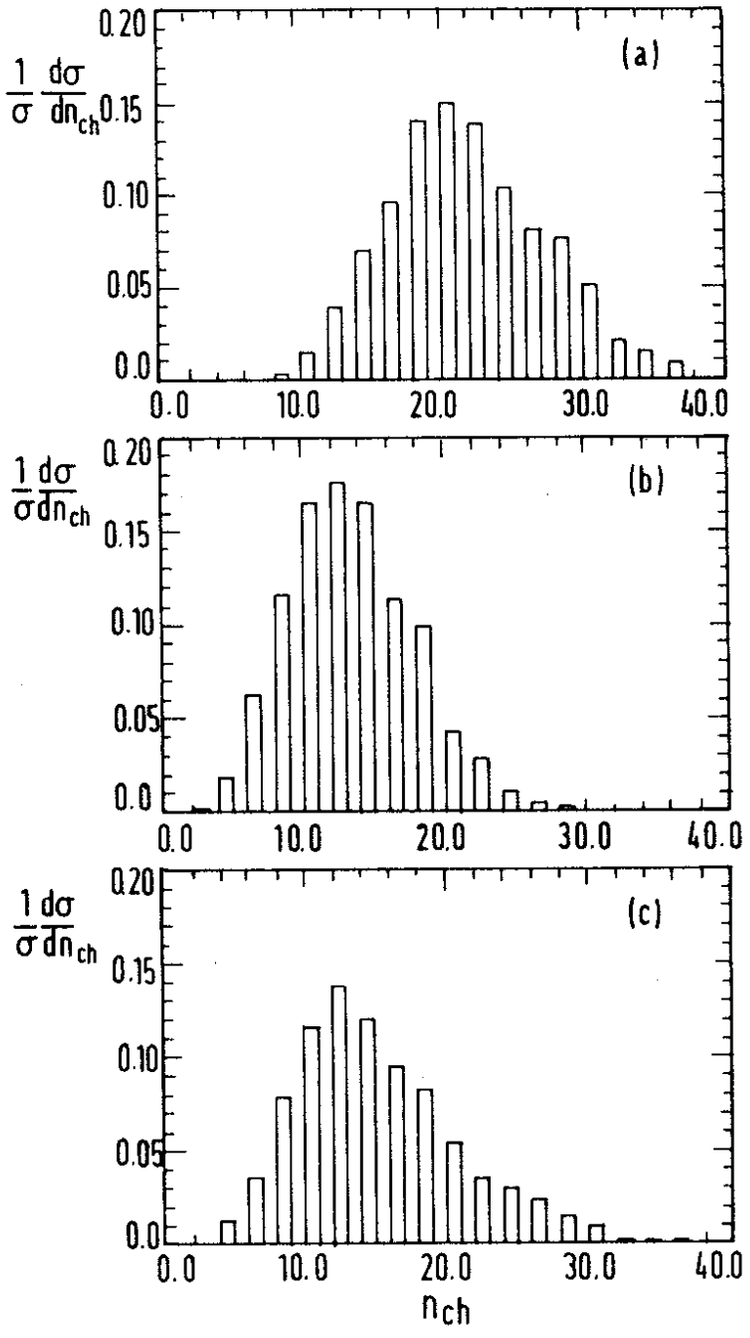
(a)
(b)
(c)
$\frac{1}{\sigma}\frac{d\sigma}{dn_{ch}}$
0.0
0.05
0.10
0.15
0.20
0.0
10.0
20.0
30.0
40.0
n_{ch}

Fig. 8

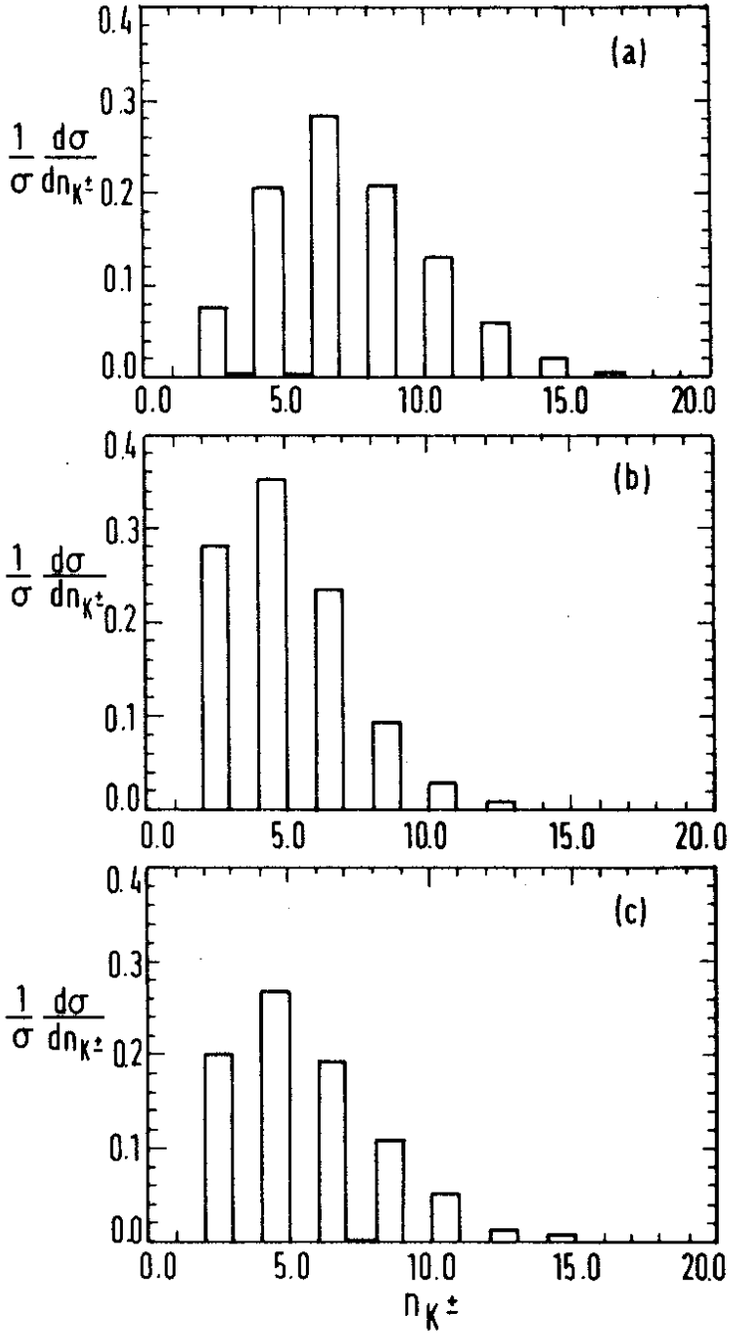
(a)
(b)
(c)
$\frac{1}{\sigma}\frac{d\sigma}{dn_{K^\pm}}$
0.0
0.1
0.2
0.3
0.4
0.0
5.0
10.0
15.0
20.0
$n_{K^\pm}$

Fig. 9

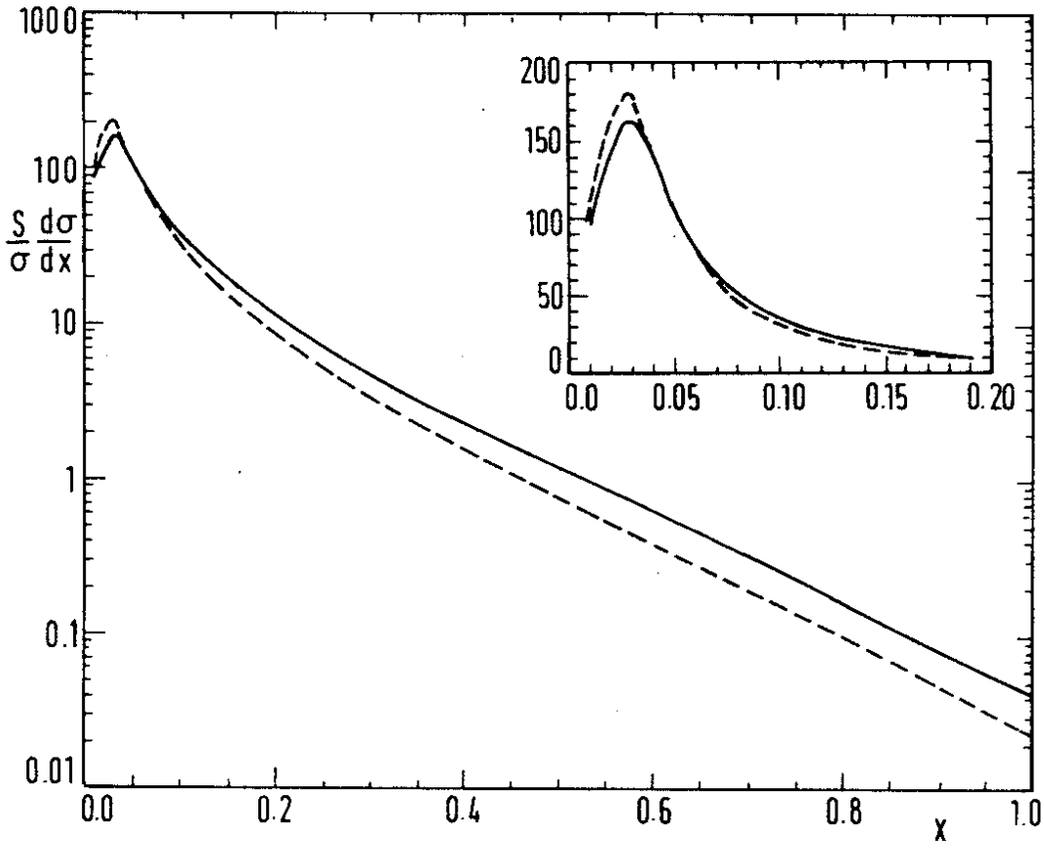
1000
100
10
1
0.1
0.01
$\frac{S}{\sigma}\frac{d\sigma}{dx}$
0.0
0.2
0.4
0.6
0.8
1.0
x
200
150
100
50
0
0.0
0.05
0.10
0.15
0.20

Fig.10

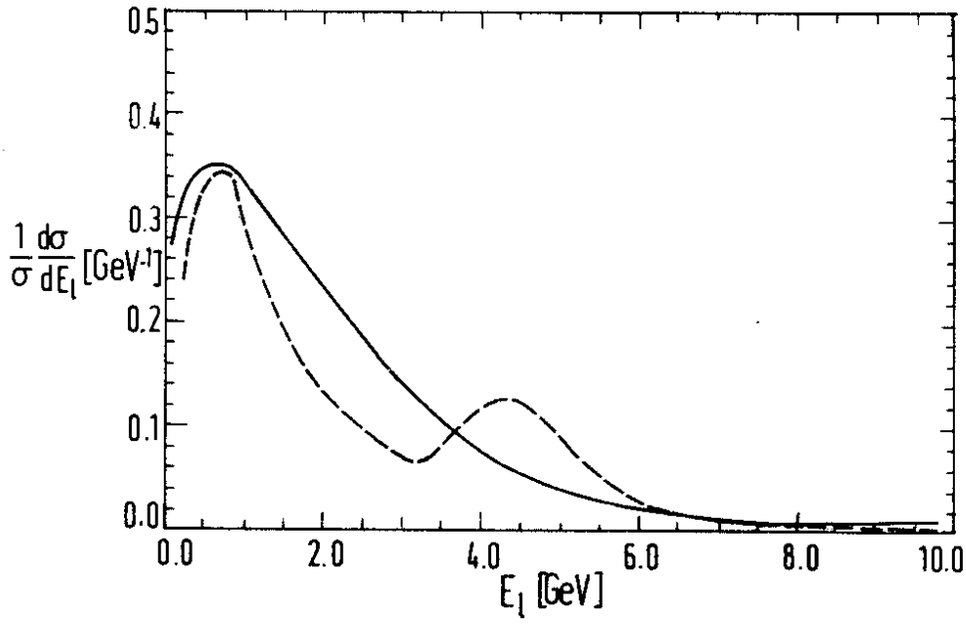
0.5
0.4
0.3
0.2
0.1
0.0
$\frac{1}{\sigma}\frac{d\sigma}{dE_l}$ [GeV^{-1}]
0.0
2.0
4.0
6.0
8.0
10.0
E_l [GeV]

Fig.11

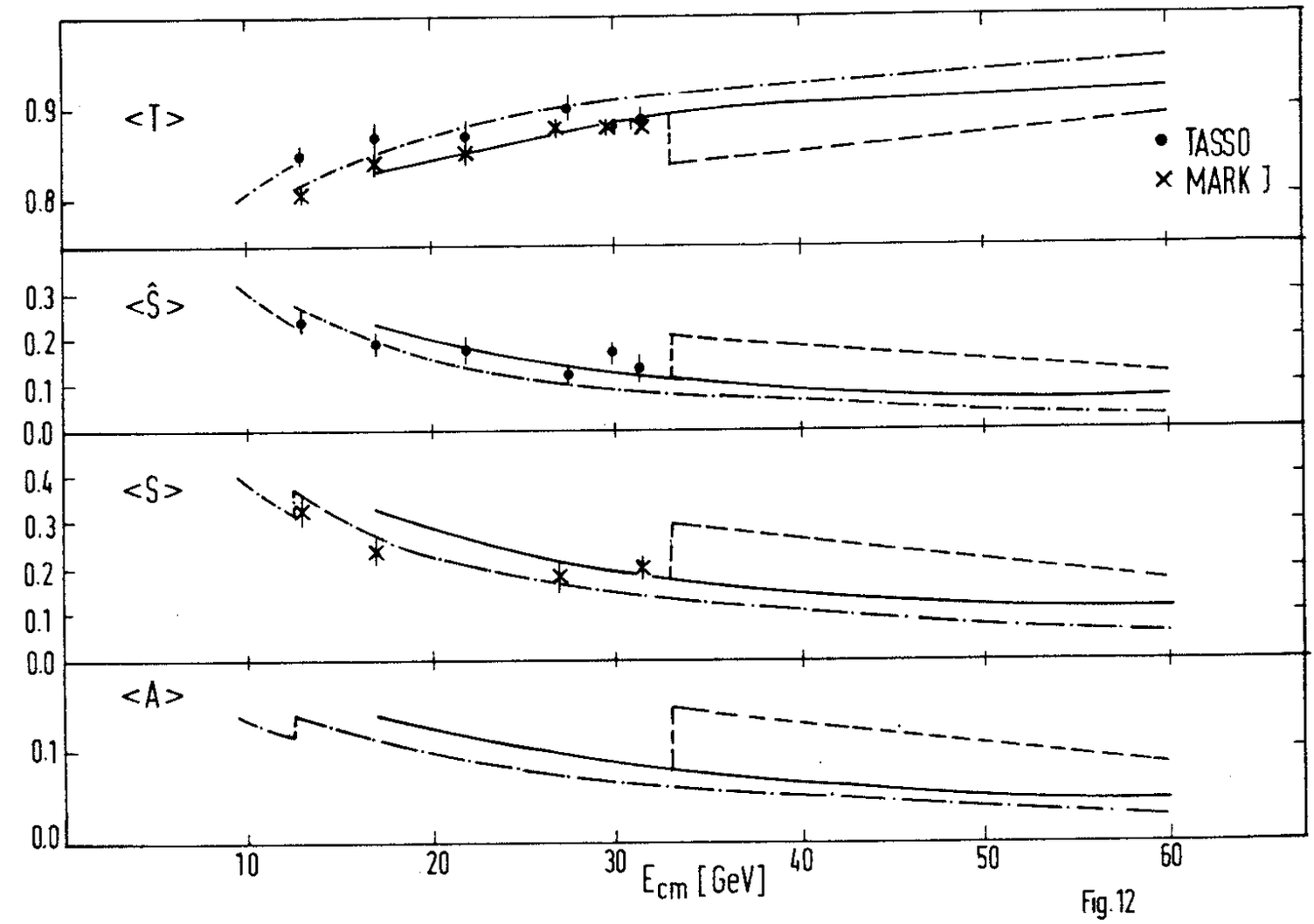
<T>
<Ŝ>
<S>
<A>
• TASSO
× MARK J
0.9
0.8
0.3
0.2
0.1
0.0
0.4
0.3
0.2
0.1
0.0
0.1
0.0
10
20
30
40
50
60
E_cm [GeV]

Fig. 12

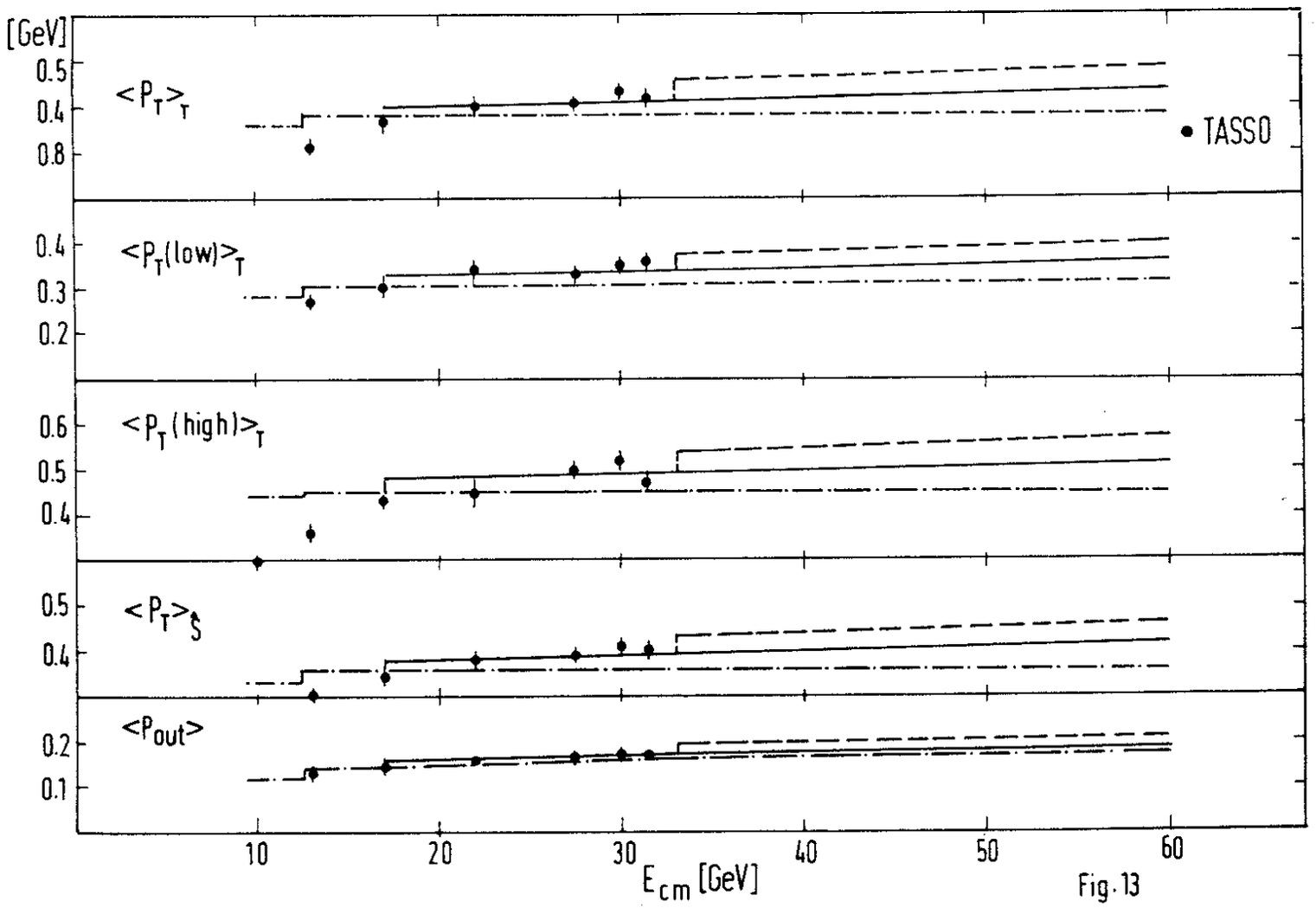
[GeV]
<P_T>_T
<P_T(low)>_T
<P_T(high)>_T
<P_T>_Ŝ
<P_out>
• TASSO
0.5
0.4
0.8
0.4
0.3
0.2
0.6
0.5
0.4
0.5
0.4
0.2
0.1
10
20
30
40
50
60
E_cm [GeV]

Fig. 13